Quaternary Science Reviews 27 (2008) 2303–2315

Contents lists available at ScienceDirect

Quaternary Science Reviews

journal homepage: www.elsevier.com/locate/quascirev

The climate in Europe during the Eemian: a multi-method approach using pollen data

S. Brewer [a,*], J. Guiot [a], M.F. Sánchez-Goñi [b], S. Klotz [c]

[a] CEREGE, CNRS/Université Paul Cézanne UMR 6635, BP 80, F-13545 Aix-en-Provence cedex France
[b] EPHE, UMR-CNRS 5805, EPOC, Université Bordeaux 1, Avenue des Facultés, 33405 Talence, France
[c] Institut für Geowissenschaften Sigwartstr. 10, D-72076 Tübingen Germany

ARTICLE INFO

Article history:
Received 22 November 2007
Received in revised form 18 July 2008
Accepted 29 August 2008

ABSTRACT

The Last Interglacial period, the Eemian, offers a testbed for comparing climate evolution throughout an interglacial with the current warm period. We present here results from climatic reconstructions from 17 sites distributed across the European continent, allowing an assessment of trends and regional averages of climate changes during this period. We use a multi-method approach to allow for an improved assessment of the uncertainties involved in the reconstruction. In addition, the method takes into account the errors associated with the age model. The resulting uncertainties are large, but allow a more robust assessment of the reconstructed climatic variations than in previous studies. The results show a traditional three-part Eemian, with an early optimum, followed by slight cooling and eventually a sharp drop in both temperatures and precipitation. This sequence is however, restricted to the north, as this latter change is not observed in the south where temperatures remain stable for longer. These variations led to marked variation in the latitudinal temperature gradient during the Eemian. The difference between the two regions is also noticeable in the magnitude of changes, with greater variations in the north than the south. Some evidence is found for changes in lapse rates, however, a greater number of sites is needed to confirm this.

1. Introduction

The Quaternary epoch is characterised by marked variations between long glacial periods and shorter interglacial periods, such as the current period, the Holocene. The previous interglacial, the Eemian, occurred between approximately 128,000 and 115,000 years before present (BP), and was characterised by temperatures that were as warm or warmer than the present (Kukla et al., 2002), and with an expansion of forests throughout the European continent. The Eemian is roughly the equivalent of oxygen isotope stage 5e, although a lag of several thousand years has been described between the start of OIS 5e and the beginning of the terrestrial Eemian records (Shackleton et al., 2003).

The interest in studying the climate during this period stems from the fact that it provides the most recent analogue for the current interglacial period. It allows the study of the climatic evolution throughout an interglacial period, and in addition, during a period with no human impact (Cheddadi et al., 1998). A second point of interest is that the orbital configuration preceding the glaciation that followed the Eemian is similar to the current configuration (Kukla and Gavin, 1992), although the amplitude of the present-day insolation change is weaker, and the duration of the period is expected to be different (Berger and Loutre, 2002).

In Europe, changes in the vegetation during this period have been studied using long pollen sequences from a wide distribution of sites (see Klotz et al. (2004), for review). In general, the early Eemian is characterised by the expansion of birch (*Betula*) and pine (*Pinus*) forests, replacing wide-spread steppic environments. The pine–birch forests were then replaced by oak (*Quercus*) forests, which, in turn, gave way to hazel (*Corylus*). The hornbeam (*Carpinus*) expanded its distribution later during the period, and the presence of this taxon is one of the main features that distinguish the Eemian from the Holocene. Following the maximum of *Carpinus*, *Picea* and *Abies* forests spread and expand. A return to pine–birch forests, with some *Picea*, marks the end of the period, and these forests eventually are replaced by steppic vegetation.

Palaeoclimate reconstructions have been made for a number of these sites (Guiot et al., 1989; Cheddadi et al., 1998; Kühl and Litt, 2003; Klotz et al., 2004) and have generally shown that the

* Corresponding author. Present address: Department of Botany, University of Wyoming, 1000 E. University Ave., Laramie, WY, 82071. USA. Tel.: +32 4 366 97 80; fax: +32 4 366 97 11.
E-mail address: brewer@cerege.fr (S. Brewer).

0277-3791/$ – see front matter © 2008 Elsevier Ltd. All rights reserved.
doi:10.1016/j.quascirev.2008.08.029

warmest and wettest conditions occur during the early part of the Eemian, followed by a gradual decrease in temperatures and reduction in precipitation. The Eemian was originally considered to be climatically stable, but recent studies have shown the occurrence of a number of abrupt, but weak amplitude, cool and/or arid events (Maslin and Tzedakis, 1996; Cheddadi et al., 1998; Sánchez-Goñi et al., 2005; Sirocko et al., 2005). A climatic analysis of the sequence from Jammertal, South Germany by Müller et al. (2005) based on high pollen counts per fossil assemblage (>2000 grains) has allowed the determination of a ~1370 years cyclic cold events during the Eemian.

These reconstructions are subject to a number of errors, including in the estimation of ages for the sequence and in the estimation of climate parameters. Sample ages are attributed by some form of interpolation between control points. For the Eemian, as sites cannot be dated using radiometric methods, the changes in the vegetation are considered to be synchronous and are used to establish correlations between sites. The climatic estimations are based on the use of transfer functions, statistical models linking climate variables and vegetation distribution. A number of different models exist, and each method explores the climate–vegetation relationship differently (Brewer et al., 2007). Variation amongst the estimations obtained is therefore representative of the uncertainty of our knowledge of this relationship.

In the current study, we attempt to reconstruct climate for 17 sites distributed across Europe (Table 1, Fig. 1), using a method that takes into account the majority of the errors associated with palaeoenvironmental reconstructions. We use a multi-method approach to the reconstruction, in order to better assess the uncertainties in the predictions, and we estimate errors linked to the chronology of each site to assess the uncertainty linked with the age-depth models. In contrast to recent Eemian studies that have largely focused on variability during this period (Cheddadi et al., 1998; Klotz et al., 2003), the goal of this study is to identify the major patterns of climate change during this period. Sánchez-Goñi et al. (2005) have shown a gradual strengthening of both vegetation and climatic gradients across Europe over the Last Glacial inception. Here, we extend this work to examine changes in this gradient throughout the Eemian on the basis of the reconstructed climatic parameters. Results are shown here as time series of climate parameters for two sites, average time series for the entire study region and as spatial distributions of climate changes for four key periods (127 ka BP, 123 ka BP, 117 ka BP and 109 ka BP).

Table 1
List of the fossil pollen diagrams used with the coordinates and references

Code	Latitude	Longitude	Elevation	Site	Reference
1	47.73	6.50	330	La Grande Pile	de Beaulieu (1977)
2	39.65	20.92	470	Ioannina	Tzedakis (1993)
3	52.05	20.97	108	Golkow	Janczyk-Kopikowa (1966)
4	50.89	16.58	175	Imbramowice	Mamakowa (1989)
5	47.06	7.51	649	Beerenmösli	Wegmüller (1992)
6	47.78	11.31	610	Eurach	Beug (1979)
7	45.23	5.58	333	Flachère	Peschke et al. (2000)
8	47.91	9.95	662	Füramoos	Müller (2000)
9	48.06	9.53	578	Jammertal	Müller (2000)
10	45.75	6.14	452	Lathuile	Hahne (unpubl.)
11	47.75	12.2	660	Samerberg	Grüger (1979)
12	50.19	6.59	423.5	Eiffel Maar	Sirocko et al. (2005)
13	50.17	6.84	402.5	Hoher List (Eiffel)	Sirocko et al. (2005)
14	45.83	5.00	267	Les Echets	Woillard (1978)
15	42.15	−9.68	0.0	MD99-2331	Sánchez-Goñi et al. (2005)
16	37.78	−10.15	0.0	MD95-2042	Sánchez-Gõni et al. (1999)
17	40.94	15.6	1326	Monticchio	Allen et al. (1999)

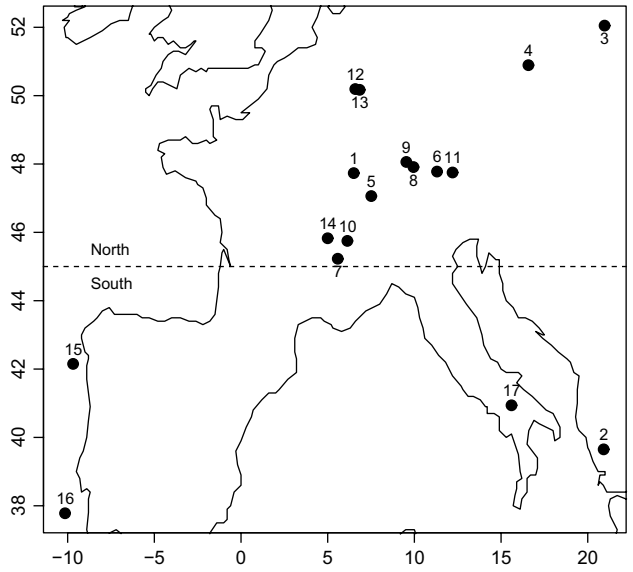

Fig. 1. Distribution of fossil sites used in the reconstruction. The numbers refer to Table 1.

2. Data

The reconstructions are based on a set of modern pollen data, covering most of the western European continent, and a series of fossil pollen sequences covering all or most of the Eemian period and subsequent transition into glacial period.

The modern data are a subset of those used by Davis et al. (2003). They are composed of 868 modern samples of 103 taxa. These samples have been grouped using the method of plant functional types (pft) (Peyron et al., 1998). The use of pfts, rather than taxa, helps to limit the problem of missing analogues of past vegetation. A set of 17 groups was retained. Six climatic variables were selected: mean temperature of the coldest month (MTCO), growing-degree-days above 5°C (GDD5, not discussed here), total annual precipitation (PREC), mean temperature of the warmest month (MTWA), mean annual temperature (TANN), ratio of actual evapotranspiration over equilibrium evapotranspiration (ALPHA, not discussed here).

The fossil data used for the climate reconstruction are taken from 17 sites with an uneven distribution across Europe (Table 1; Fig. 1). Fifteen of these are continental cores and two are marine cores (15, 16). The taxa in the fossil samples have also been grouped into 18 pft as for the modern data. The fossil sites are, however, restricted in latitude with no high latitude sites present.

3. Methods

3.1. The reconstruction techniques

We adopt a multi-method approach to better assess the error of reconstruction. We have chosen seven methods, including most standard methods used in climate reconstruction. Following ter Braak et al. (1993), the calibration is carried out between an environmental vector y (y_i, $i = 1, \ldots, n$) and a matrix of pollen assemblages X (x_{ij}, $i = 1, \ldots, n, j = 1, \ldots, m$). The subscript i (from 1 to n) represents the number of the surface samples where the m taxa are recorded (the columns of X) and where the environmental variables are to be reconstructed. The traditional equation of a transfer function can be written as follows

$$y = \sum_{j=0}^{n} b_j x_j = Xb \quad (1)$$

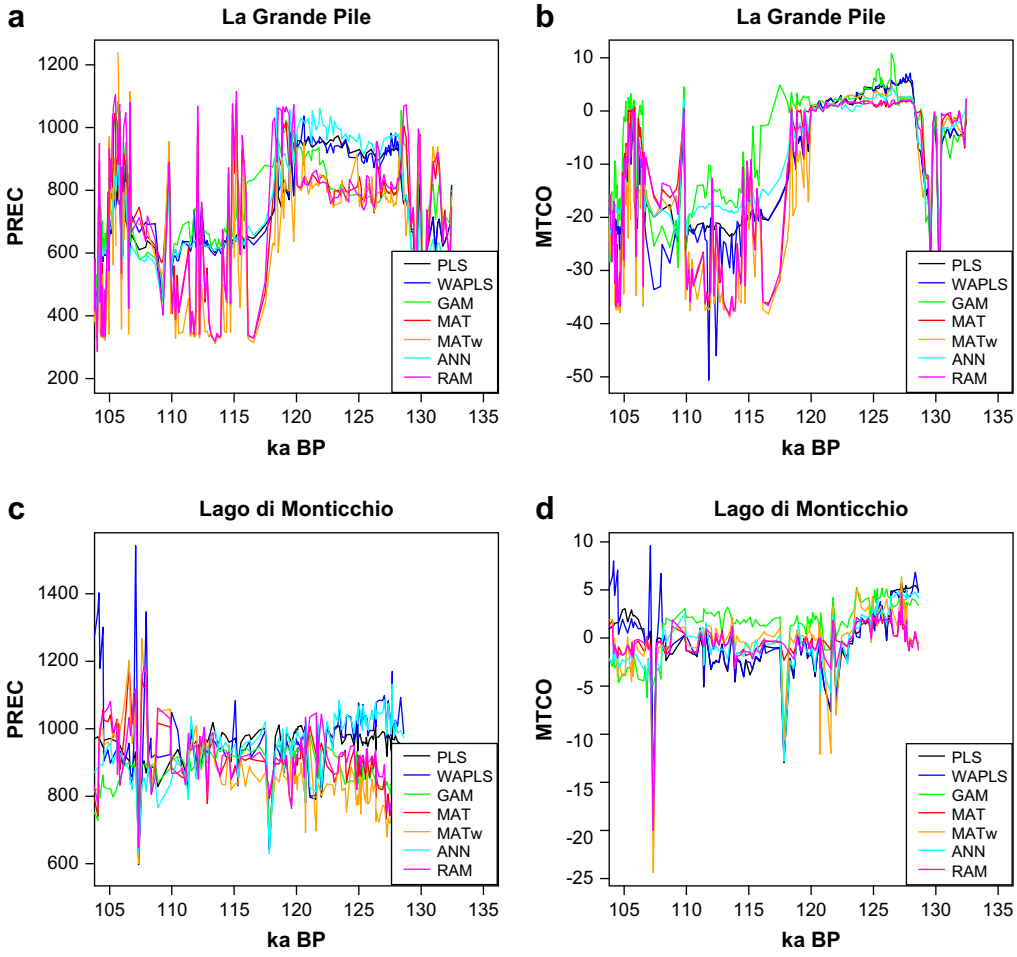

Fig. 2. La Grande Pile: reconstruction of precipitation PREC (a) and mean temperature of the coldest month (MTCO) (b) using the 7 methods. Monticchio: reconstruction of PREC (c) and MTCO (d) using the 7 methods. Horizontal axis represents the time scale in ka BP.

The first method used is partial least squares analysis (PLS). PLS maximizes the covariance between the predictand and a linear combination of the species with the condition that the norm of b is equal to 1. The quantity C to be maximized for the first component is

$$C = \frac{z'y}{b'b} \text{ where } z = Xb \tag{2}$$

z being a linear combination of the species abundance: the analysis aims to find the linear combination that maximizes the covariance with the environmental parameter. Subsequent components must be orthogonal to the first one and together.

The second method is weighted average partial least squares (WA-PLS). WA-PLS is related to correspondence analysis as PLS is related to principal component analysis (ter Braak et al., 1993). WA-PLS searches for a vector u with weighted norm equal to 1 that maximizes C:

$$C = \frac{z'Ry}{u'Ku} \text{ where } z = R^{-1}Xu \tag{3}$$

The following components are found in the same way as in the previous analyses, but with the additional condition that they are R-orthogonal. A particular case of this analysis is weighted averaging method (WA) where only one component is retained. The score u_k is then given by the average of the environmental parameters on the n observations weighted by the abundance of the kth species (this corresponds to the first factor or component). The score obtained gives an indication of where the optimum of species k occurs in the environmental domain, and y is reconstructed by averaging the m values of u_k weighted by the species abundances in the analysed sample (this corresponds to the regression).

The third method is generalized additive models (GAM) (Hastie and Tibshirani, 1990) which extends traditional regression by replacing $\sum_{i=0}^{n} b_j x_j$ in (1) by $\sum_{i=0}^{n} b_j f_j(x_j)$. Since the functions can be non-linear, GAM belongs to a non-linear family of methods. It is also a non-parametric method in the sense that it is not necessary to know the analytical form of $f_j(x_j)$. Usually, the function used is a spline function, which is very flexible and makes this model very efficient. The locally weighted regression proposed by Cleveland and Devlin (1988) fits a surface to the data in a multidimensional space by using the family of the spline functions. Gersonde et al. (2005) used GAM to estimate the sea-ice concentration from diatom assemblages during the Last Glacial Maximum (LGM, 21 ka BP).

The fourth method is also a non-linear method, artificial neural network (ANN). This consists of a number of simple and interconnected processors called neurons. A signal coming from input variables, the species assemblages, passes through these neurons to reach the output variables, the environmental variables. The interconnections are defined by coefficients which are iteratively tuned to find the best fit with the output variables. In most common use, the architecture of the ANN is composed of one hidden layer with a number of neurons, depending on the complexity of the problem. At each neuron, the incoming signal is transformed by a non-linear

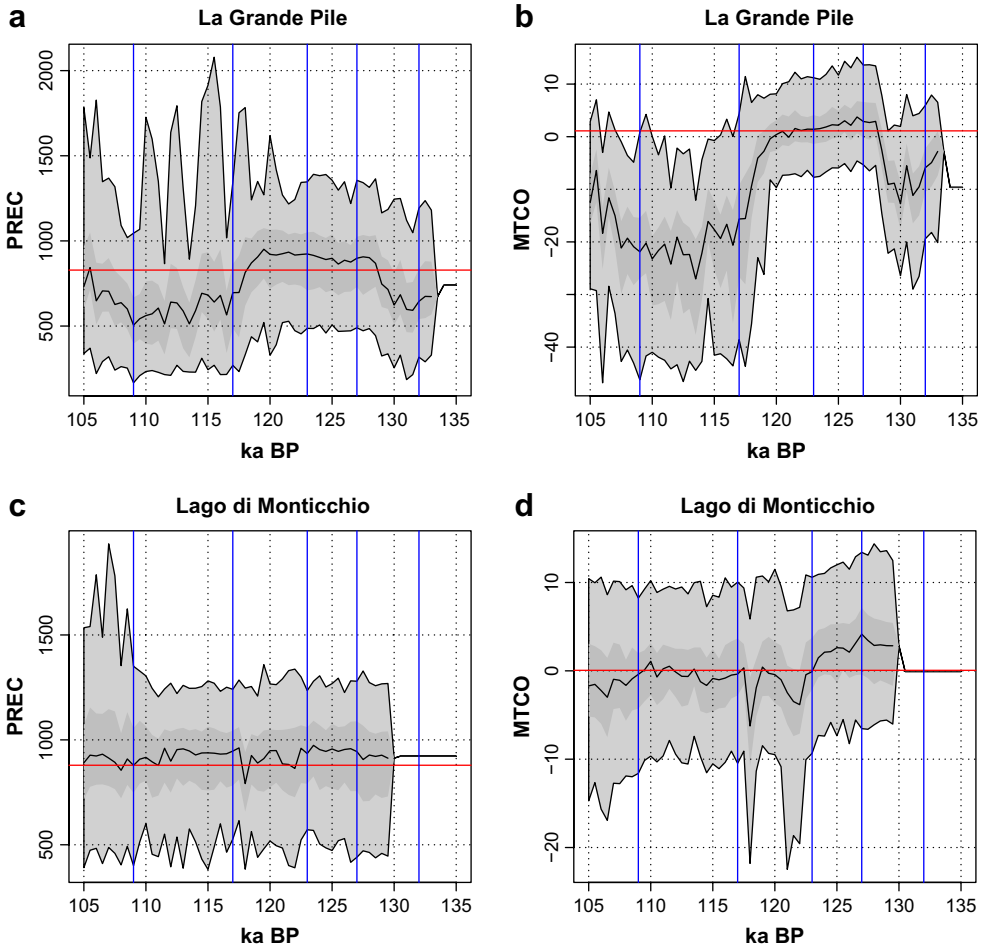

Fig. 3. La Grande Pile: summary of the reconstruction of annual precipitation (PREC) (a) and mean temperature of the coldest month (MTCO) (b). Lago di Monticchio: summary of the reconstruction of PREC (c) and MTCO (d). The dark grey zone indicates the interquartile interval taking into account the uncertainties on time scale and reconstruction (see text) and the light grey indicates the 90% confidence interval. Horizontal axis represents the time scale in ka BP. The horizontal red line indicates the modern value and the vertical blue lines indicate the time periods of interest.

function and sent to the next layer. An example of possible activation function is the sigmoid function, which translates the input in the [0, 1] domain and attenuates extreme values. This function introduces non-linearity in the model. The process of estimating the adjustable coefficients is called training. Several iterations are required for this process. One of the most commonly used ANN methods is the feed-forward network trained with the back-propagation learning algorithm. It was first used for reconstructions from pollen data by Peyron et al. (1998).

One major issue with ANN is in finding the appropriate structure of the network (number of neurons and hidden layers). No objective method exists for this, so instead a number of networks, with different designs are tested, and the most satisfying one is selected. The main guideline here is that the network chosen should be as parsimonious as possible. Another issue is the number of iterations needed during the training for correct calibration and reconstruction. It is important to stop the iterations before overestimation. Because of its non-linear property, ANN may fit the training data set very well, including the noise inherent to any data set, which can restrict its ability to make correct predictions outside of the range of the training set. To avoid such a problem, the training data set is divided into two subsets where one is used for calibration and the other is used for independent verification: when the verification error increases and becomes too large, the iterations have to be stopped. This is called early stopping.

The following methods do not require real calibration and are based on the comparison of past assemblages to modern assemblages.

The modern analogue technique (MAT) is based on the collection and analysis of a large number of modern or surface samples representing the same type(s) of sedimentary environment as the fossil samples from which microfossil assemblages have been recorded. Fossil assemblages may contain combinations of taxa that respond to different aspects of the environment. In such cases, it may be preferable to weight the taxa according to their sensitivity against the environmental variables to be reconstructed. The simplest weighting is the exclusion from the assemblages of taxa that do not display a response to any of the environmental variables being reconstructed. Another method of weighting is given by the loadings of the first principal component of the modern data (Guiot, 1990). The fifth and sixth methods used correspond to unweighted and weighted MAT reconstruction.

An appropriate distance measure is required in order to evaluate the degree of dissimilarity between fossil and modern samples. In most cases, MAT is used with microfossil data that are expressed as percentage values. It is possible to use a variety of distance measures with percentage data, with data transformations reducing the influence of ubiquitous taxa that are often more abundant in the assemblages. The most widely used distance measure is known as the chord distance, which is particularly effective with percentage

data (Overpeck et al., 1985) and may be computed using the formula below:

$$d_{ij}^2 = \sum_{k=0}^{m} \left(\sqrt{p_{ik}} - \sqrt{p_{jk}}\right)^2 \quad (4)$$

where m is the number of taxa, p_{ik} (resp. p_{jk}) is the proportion of taxon k in fossil assemblage i (resp. modern assemblage j), d_{ij}^2 is the squared chord distance between assemblages j and i. The smaller the chord distance is, the greater the degree of analogy between the two samples. Thus, paleoenvironmental reconstructions are based on a small number of modern samples that are the most similar to the fossil sample. The dispersion of the analogues around the reconstructed value provides a partial estimate of the uncertainty, which is related to the tolerance of the proxy to a relatively large range of climatic conditions. However, this estimate does not include any uncertainty related to the fitting error between the climatic conditions. A minimum distance is established by a Monte Carlo method (Guiot, 1990). We retain the 5–10 nearest analogues with a distance inferior to this minimum. If less than 5 analogues are found, no climate reconstruction is attempted for that sample.

For the weighted MAT, the taxa are weighted in (4) according to their assumed relationship to the climate. The method was proposed by Guiot et al. (1989) where the weights were obtained from the first principal component of the fossil assemblages. Here, we use the first principal component of the surface samples. With such a weighting, we hope to emphasize the importance of taxa that are coherent in space and therefore assumed to have coherent climatic controls. The method is called MATw (weighted modern analogue technique).

The final method used is the response surface method, in which the taxa are remapped into environmental space using the modern data set. The main method currently used is quantitative environmental response surfaces (Bartlein and Prentice, 1986). In this method, surfaces are fitted to the abundance values of each taxon used for reconstructions. The abundance of the taxon at each grid point can be fitted either by a flexible extrapolation technique such as locally weighted regression (Cleveland and Devlin, 1988) based on tri-cube weighting function (which is related to the GAM approach), or using inverse distance weighted interpolation (Waelbroeck et al., 1998).

Having fitted response surfaces for the suite of taxa used in reconstructions, the values for the taxa at each grid point can be combined to provide a series of assemblages that may be considered as virtual analogues. Following this, the procedure is very similar to that of MAT, with the 5 to 10 closest matching assemblages selected for each fossil assemblage and used to provide a reconstruction and a confidence interval. The dissimilarity is again conventionally measured using the chord distance.

In the response surface approach, the variation of taxa with distributions independent of climate is smoothed and thus removed by the procedure used to fit the surface. Therefore, if the principal cause of variability of a taxon is non-climatic, the response surface is flat and the taxon contributes little to the choice of analogues. As the new potential assemblages are sampled on a grid, each type of climate is evenly represented, which improves the value of the confidence intervals. These two features represent the greatest advantages of this method. We have adopted the revised analogue technique (RAM) proposed by Waelbroeck et al. (1998) where response surfaces have been used to generate new gridded assemblages and combined with original assemblages to fill the parts of the climatic space not covered by data.

3.2. Validation

Validation is an important step of the methodology. The modern sample data set is split into two. The first part is used as calibration data set and contains three-quarters of the observations and the second part is used for independent verification and contains the remaining quarter. The split is carried out as follows:

(1) the first principal component of the climatic variables is calculated
(2) the observations are sorted along the gradient of this first PC
(3) each step of 16 observations, four observations are selected for verification, so that the verification sequence is numbered (1, 2, 3, 4, 17, 18, 19, 20, 33, 34…)

This procedure is used to ensure that geographically close observations are shared between the two groups, therefore ensuring a maximum of independence of the observations. Neighbouring observations along the first PC gradient are likely to be geographically close and the selection by distant packets permits to avoid such a risk.

The first group is used as a training data set for the methods based on calibration (PLS, WA-PLS, GAM, ANN) or as a data set of potential analogues for MAT and RAM. The second group is used as an independent verification data set, i.e. the climate of this second group is estimated by using the first group. For the calibration group, the reconstructions are compared to the observed climate by calculating the root square of mean squared error (RMSE) and the determination coefficient (R^2).

$$\mathrm{RMSE} = \sqrt{\sum_{i=0}^{nc} \left(y_i - \hat{y}_i\right)^2} \quad (5)$$

For the verification group, reconstructions and observations are compared using the root square of mean squared error of prediction (RMSEP) and the reduction of error RE

$$\mathrm{RMSEP} = \sqrt{\sum_{i=0}^{nv} \left(y_i - \hat{y}_i\right)^2} \quad (6)$$

$$\mathrm{RE} = 1 - \frac{\sum_{i=0}^{nv} \left(y_i - \hat{y}_i\right)^2}{\sum_{i=0}^{nv} \left(y_i - \overline{y}_i{}^c\right)^2} \quad (7)$$

where $\hat{y}_i$ is the estimation of y_i based on the transfer function, nc is the number of observations used for calibration, nv the number of observations used for verification and $\overline{y}_i^c$ is the average of the calibration observations.

The RMSE can be considered as indicating the quality of fit of the chosen method to the modern data, whereas the RMSEP gives a measure of the error of prediction. These values depend on the relationship between pollen and data, but also the ability of the method used to capture this relationship. The confidence intervals of the predictions also take into account these problems and are larger when RMSE is large. In addition, we consider that as the different methods explore the relationship between the proxy and the climate differently, the variability of predicted values between the methods is a further indicator of uncertainty and can be added to the uncertainty of each method taken separately. Another source of error is the uncertainty from the time scale.

3.3. The time scale

As reliable radiometric dates cannot be obtained for the Eemian period and the two colder periods that surround it, each of the sequences used in this study has been dated on the basis of a set of botanical events that are found in both the continental and marine cores. The direct correlation between pollen and benthic isotopic

stratigraphies from the southwestern Iberian margin core MD95-2042 and from another deep-sea core, MD04-2845, located further north in the Bay of Biscay (work in progress), suggests these major botanical events to be synchronous despite difference in location of more than 1000 km. In this work, the marine pollen sequences have been dated, in contrast to previous studies (Shackleton et al., 2003; Sánchez-Goñi et al., 2005), by correlating the ages of methane shifts detected in ice cores with sea surface temperature changes in the mid-latitudes of the north-eastern Atlantic. It has been demonstrated that both rapid increases in methane and in sea surface temperature are contemporaneous during the last deglaciation (Severinghaus et al., 1998), and it can be assumed that this was the case during the penultimate deglaciation and the following interglacial (Waelbroeck et al., 2008). Sea surface temperature changes are in turn synchronous with vegetation changes in western Europe (Sánchez-Goñi et al., 2002). For the purposes of this study, in which we examine mean climate variation during several different periods of the Eemian, we therefore consider these events to be synchronous across all sites used here. These events are shown in Table 2.

For each site, the depth at which the event occurred was identified, and a simple age-depth chronology built using linear interpolation between samples, and an age attributed to each sample. As one aim of this study is to provide a thorough assessment of errors during the reconstruction process, the error arising during this attribution was estimated using the method proposed by Bennett (1994). At each control point, we randomly select an age from a given range, the model is fitted, and an age is estimated for each pollen sample. This is repeated 1000 times and confidence intervals are obtained by using the 5th and 95th percentile of the range of ages obtained for each pollen sample. As this method was designed for the Holocene sequences, the range of possible ages is taken from the errors arising from radiometric dating. As this information was not available here, we have used a standard range of +/− 1000 years, to account for uncertainty in the control points, and to allow for a degree of non-synchroneity between sites.

3.4. The error assessment

The originality of our approach here is to integrate all these sources of error. This is done when the reconstructions are interpolated at constant time intervals (500 years), for mapping and large-scale averages (Fig. 4). The method is as follows:

(1) for each time t, we define an interval of $t-500$ to $t+500$ years, noted I_t
(2) we consider all the samples tS_i as belonging to I_t if $tS_i + E_i \in I_t$ or I_t if $tS_i - E_i$ ∈ I_t where E_i is the error on the date; this allows the error from the age model to be taken into account
(3) for each method, the reconstructed climate of all samples S_i belonging to the interval I_t is averaged and so the confidence intervals given by the method combined into a datatset
(4) for each climatic variables, we so obtain a series of 21 values, three values (mean reconstruction MR_k, lower LS_k and upper US_k standard deviations) for each of the 7 methods (k indexes the method); these 21 values are used to define 7 half gaussian distributions of mean MR_k and standard deviations LS_k and 7 of mean MR_k and standard deviations US_k, from each 100 values are extracted randomly; the 1400 values so generated are used to defined the 5th, 25th, 50th, 75th and 95th percentiles of the reconstruction at time t.
(5) this is repeated for all climatic variables and each time interval t; time series spaced by 500 years are so obtained for each climatic variables from 135 to 105 ka BP.

Table 2
Pollen stratigraphical events used for dating by correlation with marine and ice core

Event	Date	Error
Start of *Quercus*	128.8 ka BP	1000 yr
Start of *Carpinus*	124.77 ka BP	1000 yr
Start of conifers	118.27 ka BP	1000 yr
Arboreal pollen ↘, *Artemisia* ↗	110.47 ka BP	1000 yr
2nd start of *Quercus*	106.7 ka BP	1000 yr

This method is not perfect as all the samples within the time interval are given the same weight. The weight could be dependent on the distance from the centre of I_t, however, this makes the calculations significantly more complex. In addition, the reconstruction errors of each method are not exactly equivalent, for ANN, a bootstrap error is used, for MAT or RAM, the dispersion between the analogues is used as a surrogate of the unknown error, and for the other methods, the RMSE (on the calibration data) is considered as the prediction error. However, the method does provide a framework that can account for the errors arising from the various analyses involved in climate reconstruction.

3.5. Average time series

As the aim of this study is to identify the major changes in European climate during the Eemian, we have calculated a series of average time series, based on the reconstructions taken from each site. Following studies showing that temperatures underwent different changes in northern and southern Europe during the Holocene (Cheddadi et al., 1997; Davis et al., 2003) and the latter part of the Eemian (Sánchez-Goñi et al., 2005), we have split the 17 sites at 45°N into a northern and southern set to investigate different regional changes during the Eemian. This does not give an equal split, with 13 sites in the northern set and 4 in the south. However, this division was kept as the goal was to isolate changes in Mediterranean sites from those in the centre and north of Europe, and this provides a direct comparison with the Holocene reconstructions of Davis et al. (2003).

Studies based on glacier Equilibrium Line Altitude (ELA) changes have shown evidence for a change in the temperature lapse rate (the relation between temperature and altitude) during the LGM (Mark et al., 2005). As the 17 sites included in this study include a range of elevations (0–1326 m), we have also looked for differences in climatic change according to altitude. For this, we calculated a linear relationship between temperature anomalies and site elevation for each period studied (time periods prior to 130 ka BP were ignored due to a low site density), and used changes in the slope of this relation as an index of lapse rate changes. The results are shown in Fig. 6.

Previous studies of Eemian climate change have put forward evidence for changes in the distribution of temperature, both seasonally (Cheddadi et al., 1998; Klotz et al., 2004) and spatially (Kaspar et al., 2005; Gebhardt et al., 2007) during this period. We have therefore chosen to show these changes throughout this period as an average for the European region (Fig. 5) as well as the spatial distribution of these changes for the chosen four periods (Fig. 4).

4. Results

The first part of the results gives the validation of the seven methods based on a modern sample data set split into a reference (calibration) data set of 649 spectra and a verification data set of 219 spectra. The seven methods are then applied to the 17 fossil diagrams. Reconstructions are shown for two key European sites (La Grande Pile (Woillard, 1978) and Lago di Monticchio (Allen et al., 1999)) and the variability between the different methods is

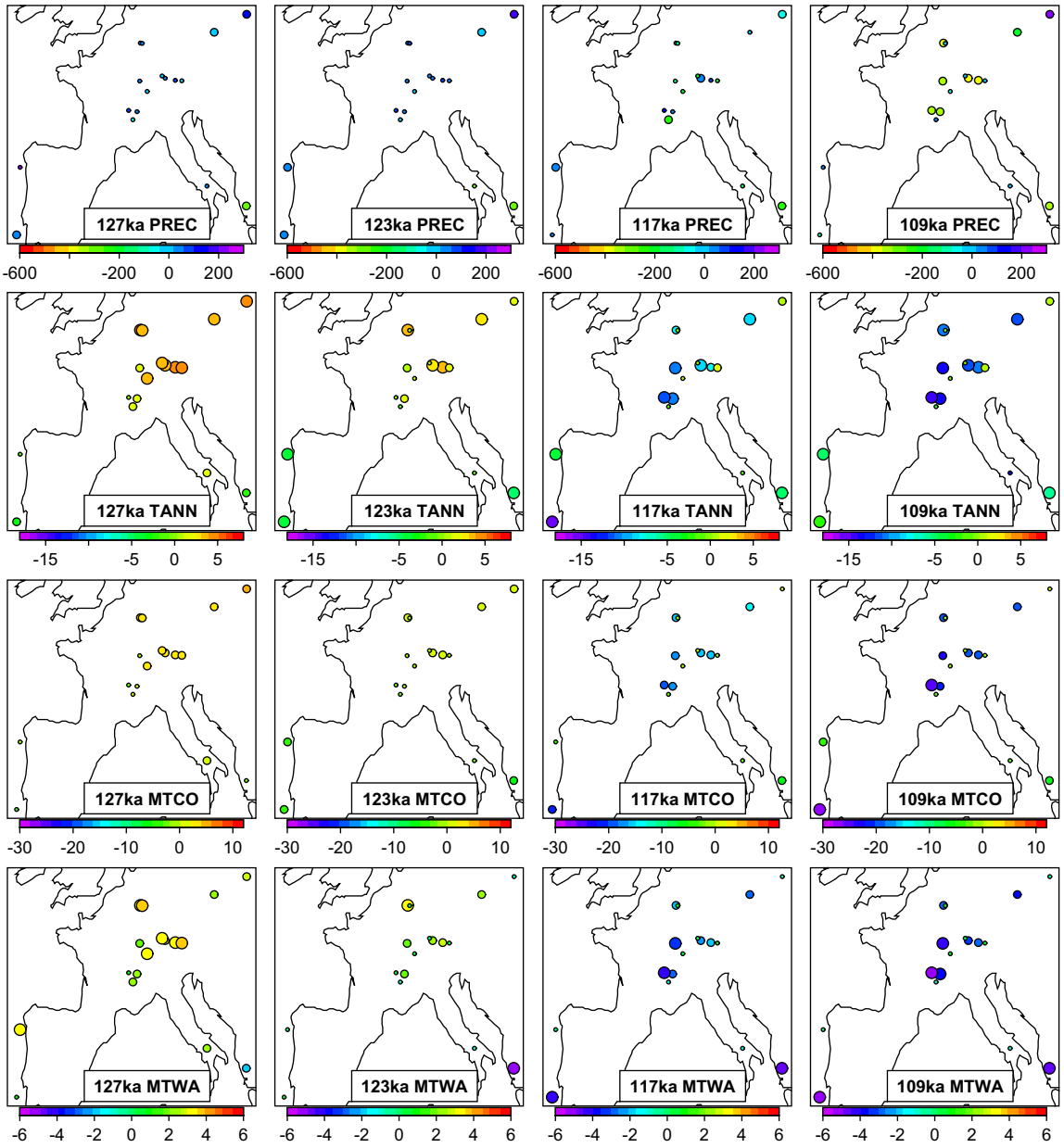

Fig. 4. Maps of four periods of the Last Interglacial for four climatic variables expressed in terms of discrepancies from the modern value. The size of the circle indicates the confidence level of the value: a dot indicates "no data", a small circle indicates that the modern value belongs to the interquartile interval (confidence < 50%), a medium circle indicates that the modern value does not belong to the interquartile interval but belongs to the 90% interval (confidence between 50% and 90%), a large circle indicates that the modern value does not belong to the 90% interval (confidence < 90%).

discussed. Finally, the results from all 17 sites are integrated at constant time intervals in order to provide a spatial analyses for several time periods and average time series for the study area.

4.1. Validation on modern data

Table 3 provides the main statistics following the validation on modern data. The calibration data set contains 648 observations and the verification data set 219 observations. A number of significant differences between the methods can be seen, both for the calibration and the validation/verification. Two methods give clearly better results than the other ones, especially for temperature: RAM and ANN. Precipitation values are generally poorly fitted with the majority of methods, except RAM, where a high R^2 (0.86) is obtained. As high precipitation (above 1000 mm) sites are quite rare in the modern data set, it is hard to reconstruct precipitation above 1000 mm. As the RAM method generates virtual samples equally distributed from 0 to 2500 mm, it is possible for this method to reconstruct very wet climates.

Another striking point is that the verification statistics are generally no worse than the calibration statistics, despite the fact that the selection of the verification data set was devised to minimize the risk of spatial correlation between the calibration and verification data sets.

4.2. The raw reconstructions

The seven methods were applied to the 17 cores of Table 1. The results are illustrated with the two selected sites (Fig. 2). Temperature reconstructions are reasonably coherent during the interglacial, but a wider spread of estimates is found during colder periods. Precipitation reconstructions are less coherent, but the

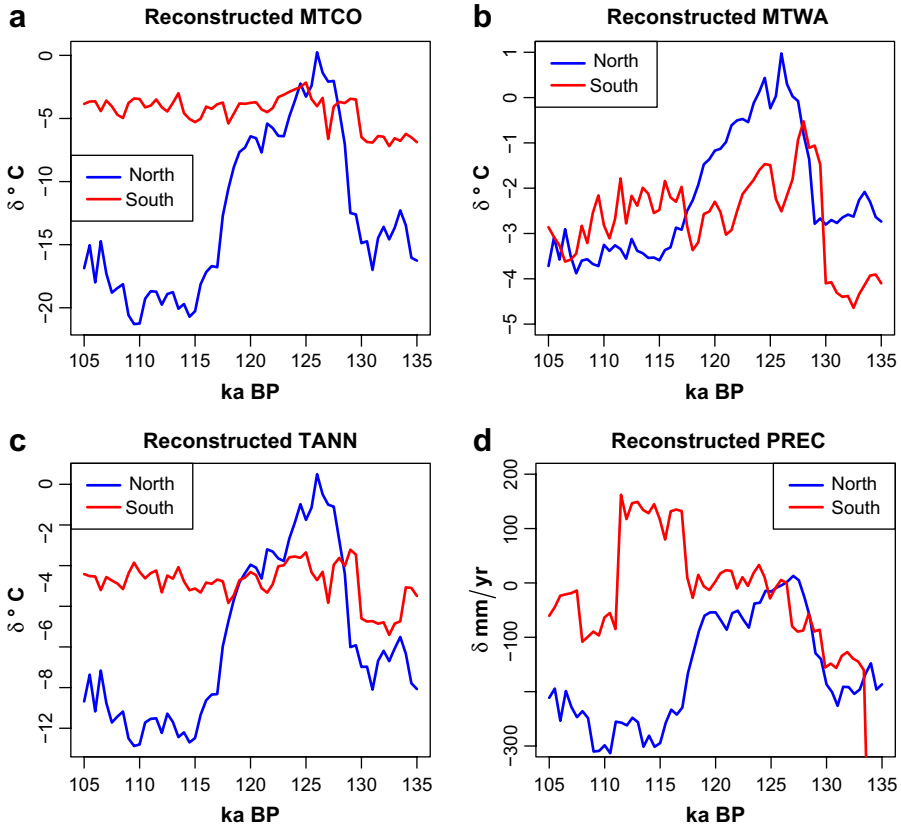

Fig. 5. Average changes in temperature and precipitation for sites in the north (>45°N) and south of Europe (<45°N). Parameters shown are (a) mean temperature of the coldest month (MTCO); (b) mean temperature of the warmest month (MTWA); (c) mean annual temperature (TANN); d) Annual precipitation (PREC).

differences during the interglacial remains similar to the uncertainties of the methods (about 200 mm, see Table 3). Generally, we can observe that the methods based on the analogues (MAT, MATw, RAM) give very close results and the other methods give also relatively clustered results. The analogue methods seem to give a larger variability in time than the other methods, especially during the cold periods. Table 4 summarizes the results by showing the mean correlation and the mean difference between each pair of methods. The mean correlations range from 0.72 to 0.91, with lower values obtained for precipitation. The spread of individual correlations between methods is relatively constrained as the minimal correlations range from 0.54 to 0.80. These correlations may hide systematic biases between the methods: for example a method may be systematically colder than another. The mean differences show that this is not true, as these mean differences are largely lower than the RMSEP of Table 3. We conclude that generally, the differences between methods are small, but they may be larger for individual samples.

4.3. Interpolation at constant time step and error assessment

At each site, all climatic variables were then interpolated onto a 500 year time step, taking into account a) the error on the time scale as indicated in Table 2; b) the uncertainty of each method; and c) the dispersion between the methods. Results for the two selected sites are shown in Fig. 3. The confidence intervals are larger for precipitation than for temperature, due to the difficulties in reconstructing this parameter. As the values for each time period are calculated as an unweighted average, the curves appear to be very smooth. The start of the sequence at the Grande Pile indicates cooler and dryer conditions prior to approximately 127 ka BP. These were followed by a humid period at both sites that lasted until 117 ka BP. During this period, temperatures decrease, slightly earlier in Italy than in France and the end of this period is characterised by cool and wet. The subsequent increase in herbaceous vegetation, is indicative of both reduced temperature and precipitation - this is shown most clearly in the Grande Pile sequence. No clear signal can be observed at Monticchio, and there is a clear difference in the results obtained by the individual methods, here the analogue methods show a positive trend while the other methods give a negative trend (Fig. 2c).

4.4. Spatial analyses

We have selected four periods: 127 ka BP, the interglacial optimum; 123 ka BP, following the optimum but with a *Carpinus* vegetation replacing the *Quercus* vegetation, 117 ka BP, after a first cooling, 109 ka BP, during the subsequent cold period. The climate anomalies for these periods have been mapped, taking into account the significance of the reconstructed change at each site (Fig. 4). A summary description of the major changes is given below. It should be noted that while the maps are rarely spatially homogeneous, some large-scale trends can be identified.

- Few of the changes reconstructed for the 127 ka BP period are significant, i.e. the change is smaller than the confidence interval. Those changes that are significant show a dryer and cooler south, and conditions close to the present in the north for both temperature and precipitation. The southern cooling appears to be dominated by changes in winter temperature, with the exception of the low latitude marine core (MD95-2042), in which little change from the present is shown.

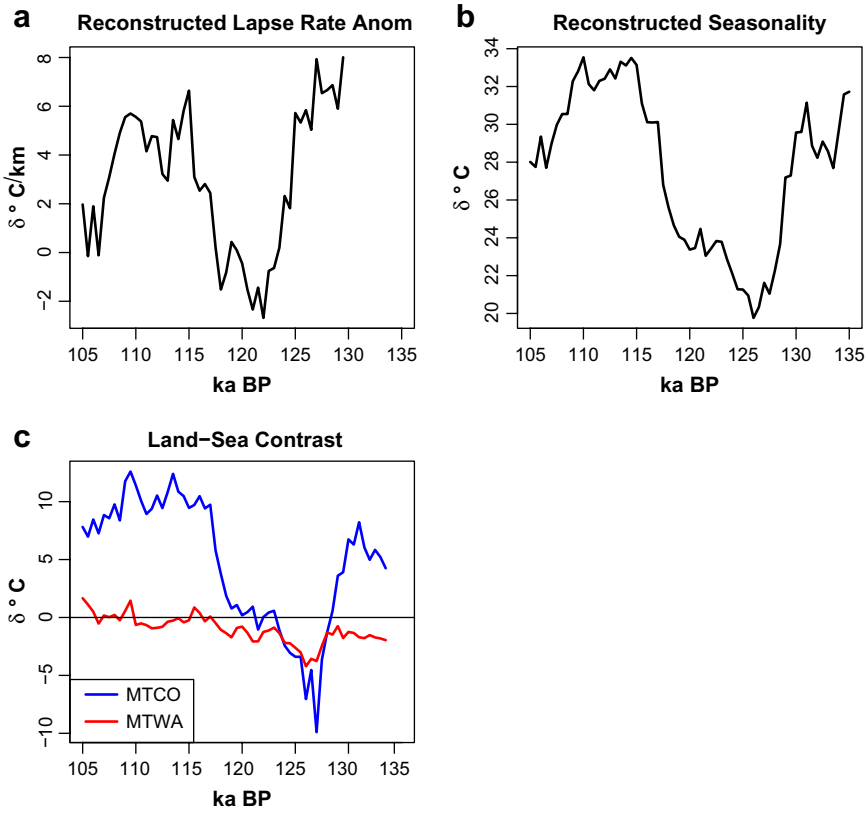

Fig. 6. a) Changes in lapse rate during the Eemian and subsequent periods averaged across all sites (*C*/km). The index is the slope of the linear relationship between annual temperature anomalies and site elevation. Positive values indicate a weakening of the lapse rate and negative anomalies a strengthening of the lapse rate. Values close to zero indicate a lapse rate close to that of today. Estimates prior to 130 ka BP have been ignored due to a low density of sites. (b) Seasonality changes for the Eemian period averaged across all sites (*C*). Seasonality is defined here as the difference between summer (MTWA) and winter (MTCO) temperatures. High values therefore correspond to a highly seasonal or continental climate, low values correspond to a less seasonal or oceanic climate. (c) Changes in the land–sea temperature contrast throughout the Eemian (*C*).

- Conditions during the 123 ka BP period remained dryer than present, but were wetter than the previous period. Precipitation decreases inland in contrast to the marine core MD95-2042, in which an increase of precipitation is estimated. This suggests a possible change in the land-sea precipitation gradient, with less water transported across the continent. The reconstructed temperatures are generally warmer than present, or similar to modern values. Exceptions to this are found throughout the Alpine region, with a marked trend towards cooling in the eastern Alps.

Table 3
RMSE and R^2 by method and by climatic variable for calibration. RMSEP and RE by method and by climatic variable for independent verification. See text for explanations

Method	GDD5	MTCO	PREC	ALPHA	MTWA	TANN
Calibration RMSE (R^2)						
PLS	1292.7 (0.62)	7.3 (0.76)	234 (0.47)	13.7 (0.73)	4.2 (0.51)	4.6 (0.76)
WA-PLS	1248 (0.65)	7.5 (0.75)	230 (0.49)	13.3 (0.75)	4.5 (0.43)	4.6 (0.76)
GAM	1138 (0.71)	7.1 (0.77)	222 (0.53)	12.2 (0.79)	3.7 (0.60)	4.2 (0.79)
MAT	1175 (0.69)	6.6 (0.81)	226 (0.51)	13.3 (0.75)	3.9 (0.56)	4.2 (0.80)
MATw	1277 (0.63)	7.6 (0.74)	239 (0.45)	14.4 (0.70)	4.2 (0.51)	4.7 (0.75)
RAM	991 (0.78)	5.3 (0.87)	250 (0.85)	11.1 (0.86)	3.6 (0.75)	3.6 (0.85)
ANN	1001 (0.77)	5.6 (0.85)	212 (0.57)	11.9 (0.80)	3.4 (0.67)	3.4 (0.87)
Verification RMSEP (RE)						
PLS	1279 (0.64)	7.1 (0.78)	202.2 (0.49)	14.1 (0.74)	4.2 (0.52)	4.5 (0.78)
WA-PLS	1348 (0.60)	8.0 (0.71)	206 (0.47)	15.3 (0.69)	4.4 (0.48)	5.1 (0.71)
GAM	1137 (0.72)	7.4 (0.76)	193 (0.54)	12.8 (0.78)	3.7 (0.64)	4.3 (0.79)
MAT	1165 (0.70)	7.1 (0.78)	229 (0.35)	13.9 (0.75)	3.7 (0.64)	4.4 (0.79)
MATw	1295 (0.63)	8.2 (0.70)	239 (0.29)	14.9 (0.71)	4.0 (0.56)	5.0 (0.72)
RAM	1089 (0.74)	5.4 (0.87)	241 (0.86)	10.1 (0.87)	3.7 (0.75)	3.9 (0.84)
ANN	982 (0.79)	5.9 (0.84)	191 (0.55)	12.4 (0.80)	3.3 (0.71)	3.4 (0.87)

- Increases in precipitation occur within the Alpine sites during the 117 ka BP period, sites at lower altitudes remain dryer than present. In the south, there is an increase in precipitation in the west and a drying in the east. A cooling occurs at all sites, with the greatest amplitude of changes in the south.
- The 109 ka BP period correspond to an interstadial (MIS 5d) and is characterised by a general change towards colder temperatures and dryer conditions in central Europe than the previous period. In southern Europe, there is a marked difference between east and west, with close to present-day temperatures and slightly wetter conditions in the west and higher continentality and reduced precipitation in the east.

4.5. Lapse rate and seasonality changes

As these estimates are based on a relatively small data set (17 sites), interpretations must be made with caution, however, two quite clear trends can be observed. The first is a period of weak lapse rates between 130 and 125 ka BP, and the second a period of

Table 4
Mean correlation, min correlation and mean differences between the seven methods for the six climate variables, based on comparison between each method and the six other methods

Variable	Mean correlation	Min correlation	Difference
GDD5	0.85	0.76	628°-days
MTCO	0.88	0.70	6.7°C
PREC	0.72	0.54	161 mm
E/PE	0.80	0.65	9.1%
MTWA	0.78	0.63	2.1°C
TANN	0.91	0.80	3.5°C

close to present or slightly stronger lapse rates, after 125 ka BP. On the basis of these results, a change in the lapse rate over the European continent occurred during the Eemian period, at approximately 125 ka BP. This change appears counter-intuitive as it corresponds to increasing precipitation, which may be expected to weaken the adiabatic lapse rate. Two possible explanations for this may be proposed: firstly, that the dryer conditions of the first period occurred mainly at low latitude sites, whereas the majority of higher altitude sites are situated in and around the Alpine chain where precipitation changes were either negligible or positive. Alternatively, the cooling is not related to lapse rate changes, but is a regional change: this earlier period corresponds to cooler conditions at sites in the south of Europe, which are at relatively lower altitudes (Fig. 2). As such it may not be possible to distinguish between a latitudinal and altitudinal temperature gradient for this period, without a greater density of sites. Subsequently, the lapse rate strengthens and returns values close or stronger than the modern value. The spatial distribution of values indicates cooling along the Alpine chain, with warming at lower altitudes, appearing to confirm an altitudinal temperature gradient. By 109 ka BP, the cooling appears to be much greater across the Alpine chain, than in the low lands, supporting a possible strengthening of the lapse rate with the start of the stadial period, this is in agreement with other lapse rate reconstructions from glacial periods (Mark et al., 2005).

The seasonality changes show marked changes with a highly seasonal or continental climate at the start of the Eemian. This is followed by an abrupt change to a period with a much reduced intra-annual temperature difference, shortly after 129 ka BP, that lasts until 120 ka BP. The climate then becomes progressively more seasonal, until it reaches pre-Eemian values by approximately 115 ka BP. Changes in seasonality appear to be largely driven by the higher amplitude MTCO changes, and it is interesting to note that these show an opposite trend to changes in seasonal insolation. This is discussed below.

5. Discussion

The available Eemian sequences vary in quality, in particular, the temporal resolution is very variable from site to site. Combining the sites by mapping or by examining large-scale trends and gradients helps to identify the major changes in Europe during the Eemian. The discussion here will therefore focus on these changes rather than any higher frequency variability.

5.1. Climate evolution during the Eemian and comparison with previous studies

5.1.1. End of Rissian glacial

The period preceding the start of the Eemian is shown here to be characterised by wide-spread colder and dryer conditions than the present day. This period has been rarely focused on in previous studies, however, where the results are available a similar pattern is shown (e.g. Cheddadi et al., 1998). Klotz et al. (2003) observed full continental conditions at a set of Alpine sites for this period, which agrees with the high seasonality shown in Fig. 6. These changes were not homogeneous: estimations of the land–sea contrast show a much weaker difference between the oceanic regions and the interior, suggesting a marked reduction in the transport of heat from the Atlantic ocean, reflecting the changes in the Gulf stream. The reduction of temperature during this period appears to be much greater in the northern part of Europe, than the south (Fig. 5). This gradient of changes is similar to that observed in reconstructions for the LGM (Peyron et al., 1998; Jost et al., 2005; Wu et al., 2007), and is likely to result directly or indirectly from the presence of high latitude ice sheets.

5.1.2. Early Eemian

The transition to the early Eemian is marked by a rapid rise in temperature and slightly slower increase in precipitation across Europe. This is one of the most characteristic features of the Eemian climate evolution and has been previously observed in a number of studies (Guiot et al., 1989; Cheddadi et al., 1998; Klotz et al., 2003; Kühl and Litt, 2003; Sánchez-Gõni et al., 1999; Sánchez-Goñi et al., 2005). The time series of anomalies presented here (Fig. 5) suggest that, despite this rapid warming, when taken as a continental average, the climate of this period was very close to modern values. This contrasts to many existing studies, in which the climate of the early Eemian is characterised as warmer and wetter than the present-day (Guiot et al., 1989; Field et al., 1994). However, as in the previous period, our results show changes during this period to be heterogeneous, with greater winter warming in the centre and north-east of Europe than in the west and north-west. Other studies of the spatial distribution of temperature changes during this period have shown similar trends in MTCO, with the largest positive anomalies around the Baltic Sea, and negative anomalies in the south (Kaspar et al., 2005; Gebhardt et al., 2007). Summer temperature changes follow a similar pattern in the results presented here, with positive anomalies occurring further inland. This is in partial agreement with the study by Kaspar et al. (2005), who show a trend of increasing positive anomalies from west to east. However, Gebhardt et al. (2007) show an opposite trend with positive anomalies centred over north-western Europe, and negative anomalies in the south east.

Kaspar et al. (2005) compared their reconstructions to temperatures simulated by the coupled ECHO-G model for the early Eemian. They obtained similar patterns of temperature change as those found here, with winter warming in north-eastern Europe and an east–west gradient of summer temperature anomalies. The origin of the changes in winter were attributed to either greater advection of warmth from the Atlantic by stronger westerlies, or by a reduction in surface albedo in the Barents Sea. At the maximum increase in temperatures in our reconstruction (at approximately 125–126 ka BP), the temperature anomaly in the south of Europe is smaller than that in the north. This indicates a weakened latitudinal temperature gradient, which although this does not agree with the hypothesis of increased westerlies proposed by Kaspar et al. (2005), may suggest that a shift in the position of these winds took place during this period, with greater advection at mid to high latitudes.

As the larger changes in temperature occur in MTCO, there is a subsequent change in seasonality during this period, with a weakening of the seasonal contrast. This switch from a highly continental climate prior to the Eemian, to an oceanic climate during the early Eemian has been previously noted by Cheddadi et al. (1998) and Klotz et al. (2003) for west-central Europe. In the Mediterranean region, the climate changes from continental or semi-desertic to Mediterranean climate (Sánchez-Gõni et al., 1999). More surprisingly, the lapse rate remains stronger than present during most of this period, although it slowly weakens towards modern values. This slow change follows the trend in precipitation (Fig. 5), which takes much longer than the temperature to reach modern values.

5.1.3. Mid-Eemian

During the mid-Eemian, characterised by the arrival of *Carpinus* at many sites, there is a general decline in temperatures. This decline is in agreement with the values obtained by Cheddadi et al. (1998), Field et al. (1994) and Rioul et al. (2001) but later studies based on a different reconstruction method show stable temperatures during this time (Klotz et al., 2003; Kühl and Litt, 2003). The difference in the results obtained has been mainly attributed to the climatic interpretation of *Carpinus* by different reconstruction methods. Methods that consider only the presence/absence of

species assign a winter optimum of 0°C to this taxon, whereas methods based on abundances assign a lower value of approximately −8°C. Kühl and Litt (2003) have suggested that the abundance of this taxon (and *Picea*, another key Eemian taxon) may be limited today due to non-climatic factors, including competition with other tree taxa.

We have attempted to limit the bias due to an inadequate set of modern analogues by using PFT scores (Peyron et al., 1998). In theory, if a given taxon is absent from a sample, it should be replaced by a taxon from the same functional group, thus reducing the no-analogue problem. Therefore a taxon that is absent or in low values in the modern data set, but abundant in fossil samples, such as *Carpinus*, will be compensated by functionally similar taxa, such as *Fagus*, that is present in the modern data, but rare in the fossil data. Changes in the abundances of functional groups are considered to be climate related, whereas changes in the dominance of taxa from the same group are ignored.

The results obtained here suggest that whilst some winter cooling took place, it was mainly restricted to the north of the continent, with southern temperatures remaining stable (Fig. 5). This difference is consistent with the north–south comparison by Sánchez-Goñi et al. (2005) who note that the first winter cooling in the south of the Iberian peninsula is later than in the north. The reduction of northerly temperatures would have led to a slight strengthening of the Latitudinal Temperature Gradient (LTG), and this period may have therefore been accompanied by increased westerlies. There is, however, little change in precipitation during this time to support this. The maps, however, indicate a more complex picture of changes, with mixed positive and negative anomalies in the north. This suggests that obtaining a clear climate signal for these pollen spectra remains problematic, due to insufficient modern knowledge, and this remains a difficult period, due to the presence of a flora that is unknown in Europe today.

5.1.4. Termination of Eemian and start of glacial

The results show that the decrease in temperatures and increasingly dry conditions that began during the Mid-Eemian continue and accelerate after approximately 120 ka BP. This is slightly later than the start of cooling recorded in GRIP (NorthGRIP Members, 2004). The decrease is consistent with the results of previous studies, although greater cooling has been found in studies based on an analogue approach (Cheddadi et al., 1998) than an indicator species approach (Klotz et al., 2003; Kühl and Litt, 2003) or oxygen isotope estimations (Rioul et al., 2001). The greater decrease in winter temperatures than summer leads to an overall increase in seasonality, supporting the return to a more continental climate as previously observed (Cheddadi et al., 1998; Rioul et al., 2001; Klotz et al., 2003; Sánchez-Goñi et al., 2005). However, this reduction appears to be restricted to the north of the continent, with little or no change observed in the south. This agrees with studies of individual sites showing that the cooling occurs nearly 5 ka later in the south (Lago di Monticchio, (Allen et al., 1999)), and the latitudinal gradient in the timing of vegetation change across Europe (Sánchez-Goñi et al., 2005). The increasing drought in the north appears to be compensated for by a stable or even increased annual precipitation in the south.

The transition to the glacial period is relatively slower than the transition out of glacial period at the start of the Eemian, suggesting that the factors driving this change are more complex. Experiments with coupled ocean–atmosphere GCMs have shown that although the decrease in insolation is insufficient to cause the observed changes, a reduction of the thermohaline circulation (Khodri et al., 2001) may have forced the inception of a glacial state. This is supported by the timing of the cooling seen in North Atlantic SST reconstructions (Cortijo et al., 1994, 1999). In particular, the reduction of summer insolation (Berger, 1978), and increased northward transport of winter moisture (Khodri et al., 2001) led to perennial sea-ice and snow cover, which then acted as a feedback to increase cooling. The increase in winter insolation appears to contradict the decrease in winter temperatures observed here, but has been shown by Crucifix and Loutre (2002) to have a weakening effect on the thermohaline circulation, thus amplifying the effect of summer cooling in the North Atlantic.

Further experiments have shown that these changes were further reinforced by feedbacks due to changes in vegetation, notably the southward shift of the treeline and replacement by tundra (Gallimore and Kutzbach, 1996; de Noblet et al., 1996; Crucifix and Loutre, 2002; Kageyama et al., 2004). The resulting increase in albedo both amplifies the effects of reduced summer insolation and helps to counter the increase in winter insolation. Kageyama et al. (2004) have shown that, in the absence of these feedbacks provided by changes in vegetation cover, ice sheets cannot develop.

5.2. Comparison with the Holocene interglacial

One of the main interests in studying the Eemian is that it provides an entire interglacial period, against which the current interglacial may be compared, including the transition into a glacial state. Here we compare some of the features of the European Eemian climate evolution against a synthetic view of European temperature change during the Holocene (Davis et al., 2003). One of the main features in both periods is an abrupt rise in temperatures at the beginning of the period. The similarity goes further in that both the seasonal differences (larger change in MTCO than MTWA) and the regional changes (larger change in north than south) are similar in the two periods. A comparison of actual values (not shown) shows that the increase in temperature at the start of each period was slightly higher during the Eemian. As the Davis et al. (2003) study starts at 12 ka BP, it may not capture all the early Holocene temperature rise. The transition between the Last Glacial period and the Holocene was marked by a series of fluctuations between interstadials and stadials (Alley, 2000). The temporal resolution of the current study is insufficient to identify such changes, however, the cold and short post-Zeifen interstadial event has been observed at certain high resolution sites (Sánchez-Gõni et al., 1999; Sánchez-Goñi et al., 2000, 2005), although a recent study of the varve sequence from Lago di Monticchio did not find any evidence for this (Brauer et al., 2007).

Following the early Holocene rise, average European temperatures remained relatively stable throughout the rest of the period. In contrast, a different and opposing evolution of temperatures was shown between the north and south (Davis et al., 2003). Differences between the north and south of Europe have also been previously noted for the Eemian (Sánchez-Goñi et al., 2000, 2005), and are confirmed here in the analysis of latitudinal differences. Fig. 5 shows positive anomalies in north during the Eemian optimum, whereas in the south, temperatures remained lower than present throughout. The distribution of anomalies during the Eemian optimum therefore resembles that observed for the mid-Holocene, with a warmer north and cooler south (Cheddadi et al., 1997; Davis et al., 2003). Unlike the Holocene, however, little change is seen in precipitation for this period.

The changing distribution of temperatures translates into a change in the LTG across Europe, with a winter gradient that is weaker during the Eemian optimum (125 ka BP) and stronger during the glacial periods and the transition to these periods (Sánchez-Goñi et al., 2005). In summer, the warming over northern Europe leads to a LTG that is much weaker than present at approximately 125 ka BP, and remains so until approximately 117 ka BP. If these changes are taken as representative of larger scale changes in the Equator–Pole gradient, they equally represent

changes in the circulation across the continent. The question remains if this north–south difference is really representative of the synoptic circulation, or is simply an artefact of the site distribution.

The reconstructed changes in the LTG shown here agree with a gradual strengthening of the equator–pole gradient of annual insolation between 125 and 115 ka BP (Crucifix and Loutre, 2002; Kaspar and Cubasch, 2007). Climate simulations for this period have equally shown a weaker summer temperature gradient for the Northern Hemsiphere at 125 ka BP and a stronger summer gradient at 115 ka BP (Kaspar and Cubasch, 2007). In both cases, the changes are mainly driven by high latitude variations. In a regional study of simulated and reconstructed Eemian climate, Kaspar et al. (2005) showed the presence of a weaker winter gradient over the European continent, although the changes in summer are less clear, due to an increased westerly flow over Europe bringing increased warmth.

5.3. Duration of the Eemian interglacial

This latitudinal difference is also noticeable in the timing of the Eemian period. If the Eemian is defined by a period of warmer temperatures following the Riss glacial period, our results show its duration to have been approximately 12 ka in the north, but somewhat longer (approx. 20 ka) in the south. The duration of the Eemian has been the subject of extensive debate (Kukla et al., 1997), which has yet to be resolved. The results presented here suggest that this problem may be due to a fundamental zonal difference in the timing of the end of the warm period. Changes in summer insolation (Berger, 1978) across this period show a reduction agreement with the reduction of temperatures in the north of Europe. However, the southern sites appear to have been buffered against this, resulting in strong climatic gradients across the continent (Fig. 5), an effect previously noted by Müller and Kukla (2004) and Sánchez-Goñi et al. (2005).

A potential mechanism for this buffer would have been a partial, rather than full reduction in the thermohaline circulation, allowing sufficient warmth to reach the south of Europe to mitigate the effects of the insolation loss. In a study of 8 marine sequences located along the path of the Gulf Stream in the North Atlantic, Cortijo et al. (1999) have shown a difference in the timing of the post-Eemian cooling, with this occurring earlier at high latitudes. This trend supports the idea of a gradual reduction in the thermohaline circulation, which would have continued to provide warmth to the south, if not the north, of the continent. Further to this, the reduction in temperatures in the north may have been amplified by the presence of perennial snow and sea-ice, with a resulting increase in albedo (Khodri et al., 2001; Crucifix and Loutre, 2002).

6. Conclusions

We have used an original multi-method approach to reconstruct the large-scale changes of climate during the Last Interglacial, the Eemian. This method takes into account the various sources of errors: time scale, various errors coming from the fact that the modern data set is not perfect, not all methods are able to correctly fit the data for a number of reasons including non-linearity, lack of analogues, etc. However, each method provides different information about the species–environment relationship and this may be used to better assess the uncertainties involved in reconstructing past climates. When all errors are taken into account, the uncertainties on the reconstructions are unsurprisingly large, and there is a certain amount of variability in the mapped values. Despite this, it is possible to identify a number of trends within the changes, by looking at the ensemble of sites.

The traditional view of an Eemian period in three parts is supported by these results: early optimum, followed by slight cooling during the *Carpinus* phase, followed by a sharp drop in temperatures and precipitation with the return of a coniferous vegetation. However, this set of changes appears restricted to the north, with a very different set of changes in south. In the south, there is a slight development of *Carpinus* at ~123 ka BP, indicating that the slight cooling reaches south to southern Iberia. Following an early rise in temperatures, the Eemian climate of the south of Europe appears to have remained warm over a long period, suggesting the insolation changes at the transition into a glacial state were buffered.

Further, the changes in the north were of a greater magnitude than in the south, in part due to a large reduction in temperatures during the glacial period preceding the Eemian, and in part due to the stability of the southern climate. These changes indicate important changes in the latitudinal temperature gradient over Europe. While similar changes are shown in winter and summer temperatures, the magnitude of the winter changes is much greater, and changes in seasonality show the Eemian to have been characterised by a highly oceanic climate in central and western Europe and a Mediterranean climate in the south, in contrast to the continental climate of the preceding and following periods.

As with the LGM, a stronger lapse rate is reconstructed in the glacial period, which gradually becomes weaker throughout the Eemian. This remains speculative, due to the low number of sites, and further data would be required to verify this.

The method proposed here has several limitations, including constant weighting of different samples in the interpolation process, or the use of different ways of calculating errors in the various individual methods. The method does, however, provide a better way to account for errors within the reconstruction process than the majority of contemporary techniques, and helps to obtain more robust estimations of past climate change.

Acknowledgements

This study was supported by the ANR project PICC. The authors thank Judy Allen for providing the pollen data for the Lago di Monticchio sequence and Ulrich Müller for Füramoos and Jammerthal data. We are grateful to Claire Waelbroeck for discussion about the new chronology of the Eemian sequences. Other data was taken from the European Pollen Database and Pangaea, and both sources are acknowledged for the services they provide. We gratefully acknowledge the comments of two anonymous reviewers, which have improved the content and clarity of this paper.

References

Alley, R.B., 2000. The Younger Dryas cold interval as viewed from central Greenland. Quaternary Science Reviews 19, 213–226.

Allen, J.R.M., Brandt, U., Brauer, A., Hubberten, H.-W., Huntley, B., Keller, J., Kraml, M., Mackensen, A., Mingram, J., Negendank, J.F.W., Nowaczyk, N.R., Oberhänsli, H., Watts, W.A., Wulf, S., Zolitschka, B., 1999. Rapid environmental changes in southern Europe during the last glacial period. Nature 400, 740–743, doi:10.1038/nature23432.

Bartlein, P.J., Prentice, I.C., 1986. Climatic response surfaces from pollen data for some eastern North American taxa. Journal of Biogeography 13, 35–57.

de Beaulieu., J.-L., 1977. Contribution pollenanalytique à l'histoire tardiglaciaire et Holocène de la végétation des Alpes méridionales françaises. PhD thesis, Univ. Aix- Marseille, 358 pp.

Bennett, K.D., 1994. Confidence intervals for age estimates and deposition times in late-Quaternary sediment sequences. The Holocene 4, 337–348.

Berger, A., 1978. Long-term variations of daily insolation and Quaternary climatic changes. Journal of Atmospheric Sciences 35, 2362–2367.

Berger, A., Loutre, M.-F., 2002. An exceptionally Long Interglacial Ahead? Science 297, 1287–1288, doi:10.1226/science.1076120.

Beug, H.-J., 1979. Vegetationsgeschichtliche pollenanalytische Untersuchungen am Riss/Würm-Intergslazial von Eurach am Starnberger See. Obb. Geologica Bavarica 80, 91–106.

ter Braak, C.J.F., Juggins, S., Birks, H.J.B., Van der Voet, H., 1993. Weighted averaging partial least squares regression (WA-PLS): definition and comparison with other methods for species–environment calibration. In: Patil, G.P., Rao, C.R. (Eds.), Multivariate Environment Statistics. Elsevier, Amsterdam, pp. 519–553.

Brauer, A., Allen, J.R.M., Mingram, J., Dulski, S., Wulf, P., Huntley, B., 2007. Evidence for last interglacial chronology and environmental change from Southern Europe. Proc. Nat. Acad. Sciences 104, 450–455, doi:10.1073/pnas.0603321104.

Brewer, S., Guiot, J., Barboni, D., 2007. Pollen data as climate proxies. In: Elias, S.A. (Ed.), Encyclopedia of Quaternary Science, vol. 4. Elsevier, pp. 2498–2510.

Cheddadi, R., Yu, G., Guiot, J., Harrison, S.P., Prentice, I.C., 1997. The climate of Europe 6000 years ago. Climate Dynamics 13, 1–9.

Cheddadi, R., Mamakowa, K., Guiot, J., de Beaulieu, J.-L., Reille, M., Andrieu, V., Granoszewski, W., Peyron, O., 1998. Was the climate of the Eemian stable? A quantitative climate reconstruction from seven European pollen records. Palaeogeography, Palaeoclimatology, Palaeoecology 143, 73–85.

Cleveland, W.S., Devlin, S.J., 1988. Locally weighted regression: an approach to regression analysis by local fitting. Journal of the American Statistical Association 83, 596–610.

Cortijo, E., Duplessy, J.C., Labeyrie, L., Leclaire, H., Duprat, J., van Wearing, T.C.E., 1994. Eemian cooling in the Norwegian Sea and North Atlantic ocean preceding continental ice-sheet growth. Nature 372, 446–449, doi:10.1038/372446a0.

Cortijo, E., Lehmann, S., Keigwin, L., Chapman, M., Paillard, D., Labeyrie, L., 1999. Changes in meridional temperature and salinity gradients in the North Atlantic Ocean (30–72N) during the last interglacial period. Paleoceanography 14, 23–33.

Crucifix, M., Loutre, M.F., 2002. Transient simulations over the last interglacial period (126–115 kyr BP): feedback and forcing analysis. Climate Dynamics 19, 417–433, doi:10.1007/s00382-002-0234-z.

Davis, B.A.S., Brewer, S., Stevenson, A.C., Guiot, J., Data contributors, 2003. The temperature of Europe during the Holocene reconstructed from pollen data. Quaternary Science Reviews 22, 1701–1716.

Field, M.E., Huntley, B.H., Müller, H., 1994. Eemian climate fluctuations observed in a European pollen record. Nature 371, 779–783.

Gallimore, R.G., Kutzbach, J.E., 1996. Role of orbitally induced changes in tundra area in the onset of glaciation. Nature 381, 503–505.

Gebhardt, C., Kühl, N., Hense, A., Litt, T., 2007. Reconstruction of Quaternary temperature fields by dynamically consistent smoothing. Climate Dynamics 143, 73–85, doi:10.1007/s00382-007-0299-9.

Gersonde, R., Crosta, X., Abelmann, A., Armand, L., 2005. Sea-surface temperature and sea ice distribution of the Southern Ocean at the EPILOG Last Glacial Maximum—a circum-Antarctic view based on siliceous microfossil records. Quaternary Science Reviews 24, 869–896.

Grüger, E., 1979. Die Seeablagerungen vom Samerberg/Obb. und ihre Stelllung im Jungpleistozän. Eiszeitalter und Gegenwart 29, 23–34.

Guiot, J., 1990. Methodology of the last climatic reconstruction in France from pollen data. Palaeogeography, Palaeoclimatology, Palaeoecology 80, 49–69.

Guiot, J., Pons, A., de Beaulieu, J.-L., Reille, M., 1989. A 140,000 year continental climate reconstruction from two European pollen records. Nature 338, 309–313.

Hastie, T., Tibshirani, R., 1990. Generalized Additive Models. Chapman and Hall.

Janczyk-Kopikowa, Z., 1966. Eemian interglacial at Golkow near Warsaw. Kwartalnik Geologiczny 10, 453–461.

Jost, A., Lunt, D., Kageyama, M., Abe-Ouchi, A., Peyron, O., Valdes, P.J., Ramstein, G., 2005. High-resolution simulations of the last glacial maximum climate over Europe: a solution to discrepancies with continental palaeoclimatic reconstructions? Climate Dynamics 24, 577–590.

Kageyama, M., Charbit, S., Ritz, C., Khodri, M., Ramstein, G., 2004. Quantifying ice-sheet feedbacks during the last glacial inception. Geophysical Research Letters 31, doi:10.1029/2004GL021339 L24203.

Kaspar, F., Kühl, N., Cubasch, U., Litt, T., 2005. A model-data comparison of European temperatures in the Eemian interglacial. Geophysical Research Letters 32 L11703.

Kaspar, F., Cubasch, U., 2007. Simulations of the Eemian interglacial and the subsequent glacial inception with a coupled ocean-atmosphere general circulation model. In: Sirocko, F., Litt, T., Claussen, M., Sánchez-Goñi, M.-F. (Eds.), The Climate of Past Interglacials, Developments in Quaternary Sciences, vol. 7. Elsevier, pp. 499–515 (Chapter 33).

Khodri, M., Leclainche, Y., Ramstein, G., Braconnot, P., Marti, O., Cortijo, E., 2001. Simulating the amplification of orbital feedbacks in the last glaciation. Nature 410, 570–574, doi:10.1038/35069044.

Klotz, S., Guiot, J., Mosbrugger, V., 2003. Continental European Eemian and early Würmian climate evolution: comparing signals using different quantitative reconstruction approaches based on pollen. Global and Planetary Change 36, 277–294.

Klotz, S., Müller, U., Mosbrugger, V., de Beaulieu, J.-L., Reille, M., 2004. Eemian to early Würmian climate dynamics: history and pattern of changes in Central Europe. Palaeogeography, Palaeoclimatology, Palaeoecology 211, 107–126.

Kukla, G., Gavin, J., 1992. Insolation regime of the warm to cold transitions. In: Kukla, G., Went, E. (Eds.), Start of a Glacial NATO ASISeries I: Global Environmental Change. Springer-Verlag, pp. 307–339.

Kukla, G., McManus, J.F., Rousseau, D.D., Chuine, I., 1997. How long was the last interglacial. Quaternary Science Reviews 16, 605–612.

Kukla, G., Bender, M., de Beaulieu, J.-L., Bond, G., Broecker, W.S., Cleveringa, P., Gavin, J.E., Herbert, T.D., Imbrie, J., Jouzel, J., Keigwin, L.D., Knedsen, K.-L., McManus, J.F., Merkt, J., Muhs, D.R., Müller, H., Poore, R.Z., Porter, S.C., Seret, G., Shackleton, N.J., Turner, C., Tzedakis, P.C., Winograd, I.J., 2002. Last Interglacial Climates. Quaternary Research 58, 2–13, doi:10.1006/qres.2001.2316.

Kühl, N., Litt, T., 2003. Quantitative time series reconstructions of Eemian temperature at three European sites using pollen data. Vegetation History and Archaeobotany 12, 205–214, doi:10.1007/s00334-003-0019-2.

Mark, B.G., Harrison, S.P., Spessa, A., New, M., Evans, D.J.A., Helmens, K.F., 2005. Tropical snowline changes at the last glacial maximum: a global assessment. Quaternary International 138-139, 168–201.

Mamakowa, K., 1989. Late Middle Polish glaciation, Eemian and early Vistulian vegetation at Imbramowice near Wroclaw and the pollen stratigraphy of this part of the Pleistocene in Poland. Acta Palaeobotanica 29 (1), 11–176.

Maslin, M.A., Tzedakis, P.C., 1996. Sultry Last Interglacial Gets Sudden Chill. Eos 77, 353–354.

Müller, U., 2000. A Late – Pleistocene pollen sequence from the Jammertal, southwestern Germany with particular reference to location and altitude as factors determining Eemian forest composition. Vegetation History and Archaeobotany 9, 125–131.

Müller, U., Klotz, S., Geyh, M., Pross, J., Bond, G., 2005. Cyclic climate changes during the Eemian interglacial in Central Europe. Geology 33, 449–452.

Müller, U.C., Kukla, G.K., 2004. North Atlantic Current and European environments during the declining stage of the last interglacial. Geology 32, 1009–1012, doi:10.1130/G20901.1.

de Noblet, N.I., Prentice, I.C., Joussaume, S., Texier, D., Botta, A., Haxeltine, A., 1996. Possible role of atmosphere–biosphere interactions in triggering the last glaciation. Geophysical Research Letters 23, 3191–3194.

NorthGRIP Members, 2004. High-resolution record of Northern Hemisphere climate extending into the last interglacial period. Nature 431, 147–151.

Peschke, P., Hannss, C., Klotz, S., 2000. Neuere Ergebnisse aus der Banquette von Barraux (Gresivaudan, franzosische Nordalpen) zur spatpleistozanen Vegetationsentwicklung mit Beitragen zur Reliefgenese und Klimarekonstruktion. Eiszeitalter und Gegenwart 50, 1–24.

Peyron, O., Guiot, J., Cheddadi, R., Tarasov, P., Reille, M., De Beaulieu, J.L., Bottema, S., Andrieu, V., 1998. Climatic reconstruction in Europe for 18,000 yr b p. from pollen data. Quaternary Research 49, 183–196.

Overpeck, J.T., Prentice, I.C., Webb, T.I., 1985. Quantitative interpretation of fossil pollen spectra: dissimilarity coefficients and the method of modern analogs. Quaternary Research 23, 87–108.

Rioul, P., Andreu-Ponel, V., Rietti-Shati, M., Batterbee, R.W., de Beaulieu, J.-L., Cheddadi, R., Reille, M., Svobodova, H., Shemesh, A., 2001. High resolution record of climate stability in France during the last interglacial period. Nature 413, 293–296.

Sánchez-Goñi, M.-F., Eynaud, F., Turon, J.L., Shackleton, N.J., 1999. High resolution palynological record off the Iberian margin: direct land–sea correlation for the Last Interglacial complex. Earth and Planetary Science Letters 171, 123–137.

Sánchez-Goñi, M.-F., Turon, J.L., Eynaud, F., Shackleton, N.J., Cayre, O., 2000. Direct land–sea correlation of the Eemian and its comparison with the Holocene: a high resolution palynological record off the Iberian margin. Geologie en Mijnbouw 79, 345–354.

Sánchez-Goñi, M.-F., Cacho, I., Turon, J.-L., Guiot, J., Sierro, F.J., Peypouquet, J.-P., Grimalt, J., Shackleton, N.J., 2002. Synchroneity between marine and terrestrial responses to millenial scale climatic variability during the last glacial period in the Mediterranean region. Climate Dynamics 19, 95–105.

Sánchez-Goñi, M.-F., Loutre, M.F., Crucifix, M., Peyron, O., Santos, L., Duprat, J., Malaizé, B., Turon, J.L., Peypouquet, J.-P., 2005. Increasing vegetation and climate gradient in Western Europe over the Last Glacial Inception (122–110 ka): data-model comparison. Earth and Planetary Science Letters 231, 111–130, doi:10.1016/j.epsl.2004.12.010.

Severinghaus, J.P., Sowers, T., Brook, E.J., Alley, R.B., Bender, M.L., 1998. Timing of abrupt climate change at the end of the Younger Dryas interval from thermally fractionated gases in polar ice. Nature 391, 141–146.

Shackleton, N.J., Sánchez-Goñi, M.-F., Pailler, D., Lancelot, Y., 2003. Marine isotope substage 5e and the Eemian Interglacial. Global and Planetary Change 36, 151–155.

Sirocko, F., Seelos, K., Schaber, K., Rein, B., Dreher, F., Diehl, M., Lehne, R., Jäger, K., Krbetschek, M., Degering, D., 2005. A late Eemian aridity pulse in central Europe during the last glacial inception. Nature 436, 833–836, doi:10.1038/nature03905.

Tzedakis, P.C., 1993. Long-term tree populations in north west Greece through multiple Quaternary climatic cycles. Nature 364, 437–440.

Waelbroeck, C., Labeyrie, L., Duplessy, J.C., Guiot, J., Labracherie, M., Leclaire, H., Duprat, J., 1998. Improving past sea surface temperature estimates based on planktonic fossil faunas. Palaeoceanography 13, 272–283.

Waelbroeck, C., Frank, N., Jouzel, J., Parrenin, F., Masson-Delmotte, V., Genty, D., 2008. Transferring radiometric dating of the Last Interglacial sea level high stand to marine and ice core records. Earth and Planetary Science Letters 265 (1), 183–194.

Wegmüller, S., 1992. Vegetationsgeschichtliche und stratigraphische Untersuchungen an Schieferkohlen des nordlichen Alpenvorlandes. Denkschriften der Schweizerischen Akademie der Naturwissenschaften 102.

Woillard, G.M., 1978. Grande Pile peat bog: a continuous pollen record for the last 140000 years. Quaternary Research 9, 1–21.

Wu, H., Guiot, J., Brewer, S., Guo, Z., 2007. Climatic changes in Eurasia and Africa at the last glacial maximum and mid-Holocene: reconstruction from pollen data using inverse vegetation modeling. Climate Dynamics 29, 211–229.